Watt-Level X-Band GaN Schottky Diode Rectifier

Xiaochen Yu[#$1], Haoran Wang[*], Xiantao Yang[#], Shawn S. H. Hsu[*], Ta-Jen Yen[^], Yejun He[&], Chaoyun Song[&], Yi Huang[#], Jiafeng Zhou[#2]

[#]Department of Electrical Engineering and Electronics, University of Liverpool, United Kingdom
[$]International Intercollegiate Ph.D. Program, National Tsing Hua University, Taiwan
[*]Institute of Electronics Engineering, National Tsing Hua University, Taiwan
[^]Department of Materials Science and Engineering, National Tsing Hua University, Taiwan
[&]College of Electronics and Information Engineering, Shenzhen University, China
{[1]xiaochen.yu, [2]zhouj}@liverpool.ac.uk

***Abstract* — This study presents the design, implementation, and performance evaluation of a watt-level 10 GHz class-F finger-type gallium nitride (GaN) Schottky barrier diode (SBD) rectifier for microwave power transfer (MPT) applications. The SBD, with an ultra-low zero-bias junction capacitance of 0.19 pF, an ultra-high breakdown voltage exceeding 150 V, a turn-on voltage of 1.24 V, and an on-resistance of 11 Ω, demonstrates exceptional performance at X-band rectification. The rectifier circuit is optimized with a class-F harmonic control network. A maximum microwave-to-DC power conversion efficiency of 61.2% is achieved at an input power of 36 dBm. These results underscore the potential of high-power GaN SBDs in enabling next-generation high-frequency and high-power MPT systems, offering significant improvements in efficiency and power handling capabilities.**

***Keywords* — high-power, microwave power transfer, GaN, Schottky barrier diode, class-F, rectifier.**

I. Introduction

Microwave power transfer (MPT) technology has been widely adopted in various applications, including satellite power systems, wireless charging infrastructure for transportation, remote surveillance solutions, energy-autonomous sensing devices, and advanced radio-frequency identification (RFID) tracking systems [1], [2]. A key component of MPT systems is the rectifier, as its microwave-to-DC conversion efficiency significantly impacts overall system performance. Most research efforts have focused on frequencies such as 0.9, 2.4 and 5.8 GHz [3]–[8], which fall within the industrial, scientific, and medical (ISM) bands, due to their broad availability and regulatory compliance.

To achieve a compact rectenna design, the selection of a higher operating frequency is crucial for reducing the size of the receiving antenna [9]. Although previous research has explored millimetre-wave frequencies, practical applications face limitations due to challenges such as lower microwave-to-DC conversion efficiency and higher system costs [10], [11]. As a result, frequency selection for MPT involves careful trade-offs, with the X-band emerging as a preferred choice. This frequency band offers an optimal balance between compact design, high efficiency, and lightweight implementation, making it well-suited for advanced rectenna systems.

In our prior research, we have concentrated on improving both the efficiency and power handling capacity of microwave rectifiers by transitioning from traditional silicon (Si) and gallium arsenide (GaAs) diodes to GaN-based diodes and HEMT [4], [12]. The exceptional material properties of GaN, including its wide bandgap characteristics (3.4 eV), high carrier concentration enabled by polarization effects, and excellent two-dimensional electron gas (2DEG) mobility at the heterointerface, make it an ideal candidate for advanced microwave diode development [13]. These attributes facilitate the realization of next-generation rectifiers capable of operating at high frequencies while delivering enhanced efficiency and robust power handling performance.

This study advances the state of the art by introducing a novel 10 GHz watt-level class-F rectifier incorporating a finger-type GaN SBD. The innovative GaN SBD architecture demonstrates superior performance characteristics at X-band frequencies, achieved through a unique combination of high breakdown voltage (V_{br}) and reduced junction capacitance (C_j). Fabrication on a GaN-on-SiC substrate yields a device with remarkable electrical properties: a turn-on voltage (V_{on}) of 1.24 V (defined at 1 mA/mm), specific on-resistance of 2.85 Ω·mm, series resistance of 11 Ω, ideality factor (n) of 1.26, and a low zero-bias junction capacitance of 0.19 pF. The diode structural design incorporates several key innovations: a y-shaped anode configuration, optimized anode-cathode spacing (L_{ac} = 1.875 μm), and advanced passivation techniques, collectively enabling a breakdown voltage surpassing 150 V. The rectifying circuit is designed using a single shunted SBD with class-F network microstrip lines, which effectively suppresses second harmonic components, thereby enhancing microwave-to-DC conversion efficiency. Validation results demonstrate a peak efficiency of 61.2% under conditions of 36 dBm input power and 470 Ω DC load. Among designs with efficiency exceeding 60%, this rectifier achieves the highest input power and demonstrates the promising capabilities of next-generation GaN-based diodes in enabling highly efficient and high-power rectification systems.

II. X-band High Power Rectifier Design

A. GaN Diode Design

Conventional diodes face significant challenges in meeting the high voltage and current requirements essential for high-power RF rectification. The inherent limitations of narrow-bandgap materials, such as silicon (Si) and gallium arsenide

(GaAs), not only constrain their efficiency but also restrict their ability to operate effectively at elevated power levels [14]. To address these constraints and improve rectification performance, SBDs with a high breakdown voltage and low junction capacitance present an effective solution. This work introduces a GaN SBD with a fingerprint configuration, designed for high-efficiency, high-power rectification.

Through optimized MOCVD (metal-organic chemical vapor deposition) processes, the GaN heterojunction structure was epitaxially deposited on a semi-insulating 4-inch silicon carbide substrate, ensuring high-quality crystal growth. The epitaxial structure consists of an aluminum nitride (AlN) nucleation layer, an iron (Fe)-doped buffer layer, a 300 nm gallium nitride (GaN) channel layer, a 16 nm aluminum gallium nitride (AlGaN) barrier layer, and a 2 nm in-situ GaN cap layer. The cross-sectional schematic and the top-view layout of the fingerprint GaN Schottky barrier diode (SBD) with RF pads are depicted in Fig. 1(a) and (b), respectively.

The device fabrication process commenced with the recess of the Ohmic region, defined through lithography and chlorine-based inductively coupled plasma (ICP) etching. Subsequently, an optimized titanium/aluminium (Ti/Al) metal stack was deposited using an electron-beam (E-gun) evaporation system, followed by rapid thermal annealing (RTA) at 825 °C for 30 seconds in a nitrogen (N_2) ambient, resulting in a cathode length (L_c) of 25 μm, ohmic contacts were then formed on the semiconductor surface. Device isolation was accomplished via multiple-energy boron ion implantation, which precisely defined the active region. Subsequently, a SiN_x passivation layer was grown via PECVD (plasma-enhanced chemical vapour deposition) at 300°C, effectively suppressing surface states through optimized deposition conditions. The Y-shaped anode feet were patterned using ICP etching, with an anode length of 0.25 μm (L_a) and a head width of 0.35 μm. Finally, RF pads were fabricated to facilitate on-wafer RF measurements, compatible with 100 μm pitch ground-signal-ground (GSG) probes.

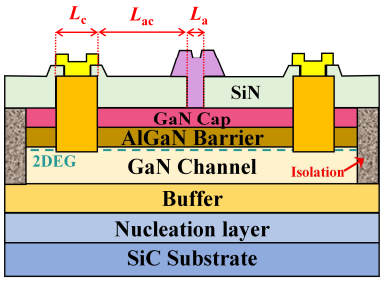

(a)

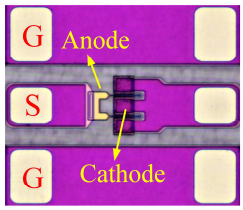

(b)

Fig. 1. (a) Cross-sectional schematic of the GaN SBD. (b) Top view of the finger-type GaN-on-SiC diode with GSG pads.

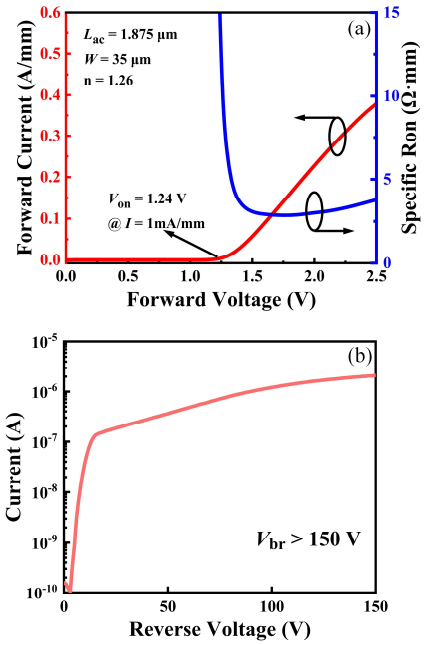

Fig. 2. *I-V* characteristics of fingerprint GaN SBD. (a) Forward current and specific turn-on resistance. (b) Reverse condition with V_{br} exceeding 150 V.

Fig. 2(a) illustrates the DC characteristics of a two-finger SBD with a finger width W=35 μm and an anode-cathode separation L_{ac}=1.875 μm. The device exhibits a forward current density of 385 mA/mm at a forward voltage of 2.5 V, with a specific on-resistance of 2.85 Ω·mm. The turn-on voltage (V_{on}), defined at a forward current of 1 mA/mm, is measured to be 1.24 V, accompanied by an ideality factor (n) of 1.26 and a Schottky barrier height of 1.02 eV, as extracted from the analysis.

Fig. 2(b) depicts the reverse current-voltage (*I-V*) characteristics, demonstrating a high breakdown voltage (V_{br}) exceeding 150 V. Notably, the reverse voltage remains stable (over 90 V) even at a reverse current of 10 μA, indicating excellent device reverse characteristics. Furthermore, the junction capacitance is measured to be 0.19 pF under zero-bias conditions.

B. Class-F Rectifying Circuit Design

The schematic of the X-band Class-F GaN SBD power rectifier is depicted in Fig. 3(a), and the detailed electrical parameters of the transmission lines are listed in Table 1. The basic parameters of the GaN SBD are V_{on} of 1.24 V, R_s of 11 Ω, C_j of 0.19 pF, and V_{br} exceeding 150 V. The fabricated rectifier, as shown in Fig. 3(b), comprises an impedance matching circuit (TL1-TL3), the GaN SBD, a class-F network (TL4-TL6), a DC filter and a load. The dimensions of certain transmission lines are slightly adjusted based on the electromagnetic (EM) simulation results obtained from the Advanced Design System (ADS). The impedance-matching circuit is designed to transform the input impedance of the circuit to 50 Ω, ensuring optimal power transfer. Additionally, the DC filter recycles the RF energy to improve power conversion efficiency. To minimize matching losses, a Rogers

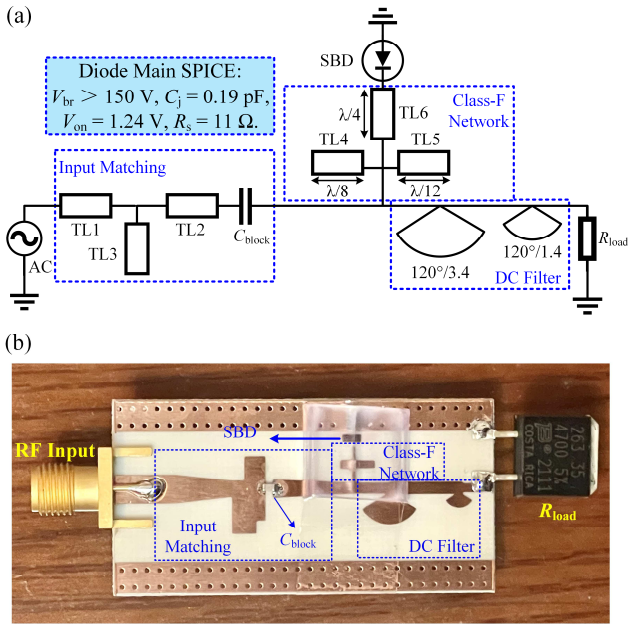

Fig. 3. (a) Circuit configuration of the developed class-F rectifier with detailed SPICE parameter. (b) Photographic of the fabricated X-band class-F rectifier circuit.

Table 1. Microstrip lines electrical parameters.

	TL1	TL2	TL3	TL4	TL5	TL6
Z_0 (Ω)	50	120	15.9	50	50	50
Elec. Length	50°	36.7°	46.3°	45°	30°	90°

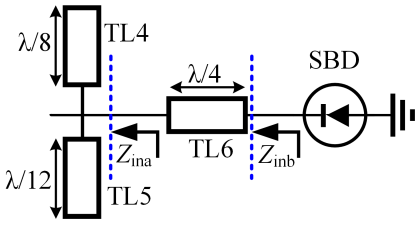

Fig. 4. Input impedance characteristics of the class-F harmonic network.

3003 substrate is employed, characterized by a dissipation factor of 3.00, tan D of 0.0010 at 10 GHz, and thickness of 1.6 mm is selected to reduce the matching loss.

The proposed harmonic termination network is composed of multiple transmission lines meticulously engineered to regulate impedance characteristics across various harmonic frequencies. The key components of the network are TL4, TL5 and TL6, with electrical lengths of $\lambda/8$, $\lambda/12$ and $\lambda/4$ at the fundamental frequency, respectively (Fig. 4). The impedance at Z_{ina} is primarily dictated by the impedance transformation properties of TL4 and TL5. Specifically, at the second harmonic, TL4, being an open-ended $\lambda/8$ transmission line, transforms into a short circuit, resulting in $Z_{ina} = 0$. Concurrently, at the third harmonic, TL5, functioning as an open-ended $\lambda/12$ transmission line, similarly transforms into a short circuit, thereby ensuring Z_{ina} remains at 0. The impedance at Z_{inb} is predominantly influenced by TL6, which possesses an electrical length of $\lambda/4$ at the fundamental frequency. The transformation process of TL6 can be elucidated as follows: at the second harmonic, given that $Z_{ina} = 0$, TL6 effectively functions as a $\lambda/2$ transmission line. This maintains the impedance characteristics of its termination, thereby directly transferring the short circuit at Z_{ina} to Z_{inb}, yielding $Z_{inb} = 0$. At the third harmonic, with Z_{ina} still at 0, TL6, now exhibiting an electrical length of $3\lambda/4$, is equivalent to a $\lambda/4$ transmission line due to its periodic impedance transformation property. This equivalence implies that a $\lambda/4$ transmission line inverts the input impedance. Consequently, the short circuit at Z_{ina} is transformed into an open circuit at Z_{inb}, leading to $Z_{inb} = \infty$. This impedance control mechanism ensures selective harmonic terminations, which play a critical role in improving the performance of rectifier circuits and high-efficiency power conversion systems.

The rectification efficiency (η) is calculated using the following formula: $\eta = (V_{out}^2/R_{load})/P_{in}$, where V_{out} and P_{in} are the output voltage and input power, respectively.

The simulated and measured rectification efficiency at 10 GHz is shown in Fig. 5. The rectifier achieves a maximum efficiency of 61.2% at 36 dBm. The efficiency is greater than 50% over an input power range of 20 to 38 dBm, with a wide power dynamic range of up to 18 dB.

In comparison to state-of-the-art X-band rectifiers utilizing Si, GaAs, and GaN SBDs as well as GaN field-effect transistors (FETs) [15]–[19], as summarized in Table 2. Among X-band rectifiers with efficiencies exceeding 60%, the proposed GaN-based rectifier achieves the highest input power level. demonstrates superior performance, particularly in terms of efficiency across the peak input power.

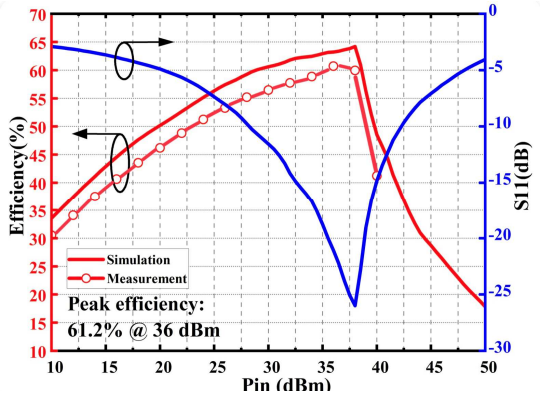

Fig. 5. Electromagnetic simulation results: RF-to-DC power conversion efficiency and S11 parameters of the rectifier versus varying RF input power levels.

Table 2. Comparisons with other X-band designs.

Refs.	Freq (GHz)	Circuit	η_{peak}	Pin (dBm)
[15]	9.6	Si diode	63%	26
[16]	X-band	Si diode	72.2%	19.4
[17]	12.75	GaAs diode	45%	20
[18]	10	GaN diode	80.1%	25.2
[19]	9.9	GaN FET	52%	39
This work	10	GaN diode	61.2%	36

III. Conclusion

This study presents the design and implementation of a high-power, high-efficiency 10 GHz Class-F rectifier utilizing a newly developed GaN Schottky barrier diode (SBD). The diode exhibits exceptional performance characteristics, including a high breakdown voltage exceeding 150 V and a low zero-bias junction capacitance of 0.19 pF, enabling superior power handling capabilities in the X-band frequency range. By integrating harmonic compression microstrip lines, the rectifier achieves a peak RF-to-DC conversion efficiency of 61.2% at an input power of 36 dBm. These results underscore the significant potential of the proposed GaN diode for advancing high-efficiency, high-power rectifiers and MPT applications in future wireless systems.

References

[1] Kim, Dowon, Ahmed Abu-Siada, and Adrian Sutinjo. "State-of-the-art literature review of WPT: Current limitations and solutions on IPT." *Electric Power Systems Research* 154 (2018): 493-502.

[2] X. Yang, X. Yu, M. Liu, K. Kurskiy, S. Shen and Y. Huang, "A Passive 3D Beam-Steering Gravitational Liquid Dielectric Resonator Antenna with Polarization Diversity," in *IEEE Transactions on Antennas and Propagation*, doi: 10.1109/TAP.2025.3544932.

[3] J. Guo and X. Zhu, "Class F rectifier RF-DC conversion efficiency analysis," 2013 *IEEE MTT-S International Microwave Symposium Digest (MTT)*, Seattle, WA, USA, 2013, pp. 1-4, doi: 10.1109/MWSYM.2013.6697776.

[4] X. Yu et al., "Sensitive Microwave Rectifier for High-Power Wireless Transfer Based on Ultra-Low Turn-On Voltage Quasi-Vertical GaN SBD," in *IEEE Open Journal of Power Electronics*, vol. 5, pp. 1756-1766, 2024, doi: 10.1109/OJPEL.2024.3490614.

[5] Y. Lee, S. Bae, S. Bin, Y. C. Choi, W. Lim and Y. Yang, "2.08 GHz GaN Doherty Rectifier with 20 dB Input Dynamic Range," *2024 54th European Microwave Conference (EuMC)*, Paris, France, 2024, pp. 461-464, doi: 10.23919/EuMC61614.2024.10732491.

[6] X. Yu, J. Zhang, M. Liu, Y. Huang, T. -J. Yen and J. Zhou, "Ultra Wide Dynamic Range High Power RF Rectifier," *2024 18th European Conference on Antennas and Propagation (EuCAP)*, Glasgow, United Kingdom, 2024, pp. 1-4, doi: 10.23919/EuCAP60739.2024.10501749.

[7] S. A. morabetil, M. RIFI, H. Terchoune and J. Zbitou, "High Efficiency Rectifier Circuit For Ambient RF Energy Harvesting Applications At 5.8 Hz," *2019 7th Mediterranean Congress of Telecommunications (CMT)*, Fez, Morocco, 2019, pp. 1-5, doi: 10.1109/CMT.2019.8931352.

[8] McSpadden, James O., Lu Fan, and Kai Chang. "Design and experiments of a high-conversion-efficiency 5.8-GHz rectenna." *IEEE Transactions on Microwave Theory and techniques* 46.12 (1998): 2053-2060.

[9] Balanis, Constantine A. *Antenna theory: analysis and design*. John wiley & sons, 2015.

[10] Gao, Si-Ping, Hao Zhang, and Yong-Xin Guo. "Analysis of mmwave rectifiers with an accurate rectification model." *2021 IEEE Wireless Power Transfer Conference (WPTC)*. IEEE, 2021.

[11] Y. Fang, W. Hong and H. Gao, "Analysis of mm-Wave Multi-Stage Rectifier and Implementation," in *IEEE Transactions on Microwave Theory and Techniques*, vol. 70, no. 10, pp. 4491-4501, Oct. 2022, doi: 10.1109/TMTT.2022.3197755.

[12] Yu, Xiaochen, et al. "Dual-Module Ultrawide Dynamic-Range High-Power Rectifier for WPT Systems." *Energies* 17.11 (2024): 2707.

[13] Carneiro, Elodie. *Optimization of GaN on Silicon technology for RF power applications*. Diss. Université de Lille, 2024.

[14] Wang, Haoran, et al. "Low turn-on voltage and high breakdown GaN Schottky barrier diodes for RF energy harvesting applications." *Japanese Journal of Applied Physics* 59.SG (2020): SGGD12.

[15] L. Cao, X. Lin and S. Liu, "Design of a High Conversion Efficiency X-Band Rectenna for Microwave Power Transmission," *2020 9th Asia-Pacific Conference on Antennas and Propagation (APCAP)*, Xiamen, China, 2020, pp. 1-2, doi: 10.1109/APCAP50217.2020.9245994.

[16] F. Tan and C. Liu, "Design of a High-Conversion-Efficiency X-Band Rectifier for Microwave Wireless Power Transmission," *2018 International Conference on Microwave and Millimeter Wave Technology (ICMMT)*, Chengdu, China, 2018, pp. 1-3, doi: 10.1109/ICMMT.2018.8563898.

[17] B. Hu et al., "A Ku-Band Microwave Wireless Energy Transmission System Based on Rectifier Diode," in *IEEE Access*, vol. 7, pp. 135556-135562, 2019, doi: 10.1109/ACCESS.2019.2942562.

[18] K. Dang et al., "Self-Aligned and Low-Capacitance Lateral GaN Diode for X-Band High-Efficiency Rectifier," in *IEEE Electron Device Letters*, vol. 43, no. 4, pp. 537-540, April 2022, doi: 10.1109/LED.2022.3154589.

[19] S. Schafer, M. Coffey and Z. Popović, "X-band wireless power transfer with two-stage high-efficiency GaN PA/ rectifier," 2015 *IEEE Wireless Power Transfer Conference (WPTC)*, Boulder, CO, USA, 2015, pp. 1-3, doi: 10.1109/WPT.2015.7140186.